Available online at www.sciencedirect.com
SCIENCE DIRECT®
Catalysis Today 105 (2005) 421–428
CATALYSIS TODAY
www.elsevier.com/locate/cattod

Fast gas–liquid–solid reactions in monoliths: A case study of nitro-aromatic hydrogenation

Michiel T. Kreutzer *, Freek Kapteijn, Jacob A. Moulijn

Reactor and Catalysis Engineering, DelftChemTech, Faculty of Applied Sciences, Delft University of Technology, Julianalaan 136, 2628 BL Delft, The Netherlands

Available online 12 July 2005

Abstract

Monolith catalyst supports are attractive as fixed bed reactors that, at the scale of the catalyst dimension, exhibit the mass transfer characteristics of slurry reactors. This paper presents a reactor design study for the single-pass conversion of dinitrotoluene in a loop configuration with an external heat exchanger. The advantage of such a loop system is the elimination of a solvent, which in turn allows more reaction heat to be recovered. The advantages of using a monolith are the low pressure drop at high recycle ratio, while maintaining good mass transfer characteristics. The modelling includes internal diffusion limitation, external mass transfer characteristics, heat effects, maldistribution and flow stability. The optimal design is found at the lowest hydrodynamic stable flow rates, where the mass transfer is fastest and the residence time in the column maximal.

Keywords: Structured reactors; Monoliths; Dinitrotoluene; Multiphase reactors; Modelling

1. Introduction

Monolith reactors have been shown to have good mass transfer characteristics, low pressure drop, and little backmixing [1]. In this work, a design for a monolith reactor is presented for the hydrogenation of 2,4-dinitrotoluene (24DNT) to 2,4-toluenediamine (24TDA). This process was selected as a case study for several reasons: (1) there is industrial interest in using monoliths for this process [2], (2) it is a fast reaction, which benefits from the good mass transfer characteristics, (3) plug flow behaviour reduces the required reactor volume and (4) the low pressure drop is advantageous, as will be explained later on.

The hydrogenation of 24DNT to 24TDA is highly exothermic ($\Delta H_R = -550$ kJ/mol per nitro-group converted), and removal of heat is the primary concern in the design of the process. Typically, stirred tank slurry reactors with internal cooling are used on a commercial scale for the process, and the dinitrotoluene is introduced into this reactor at concentrations of 5–15 mol/m^3 along with a solvent. The solvent – generally water, aliphatic alcohols or mixtures thereof – serves two purposes. Without dilution by solvent the high concentration of dinitrotoluene results in too high reaction rates. Further, the temperature rise of the reaction medium may be moderated by evaporation of the solvent. For a modelling study of 24DNT hydrogenation in a stirred reactor with an evaporating solvent, see e.g. Janssen et al. [3].

The slurry reactor process has several disadvantages: (i) the solvent has to be removed from the product. This problem can be overcome by using the product 24TDA as the solvent. (ii) The fine catalyst powder has to be filtered out of the product. Potential solutions are the use of a filter inside the reactor or the use of a fixed bed reactor. Chimerol et al. [4] disclosed a stirred tank reactor employing a filter inside the reactor, such that the catalyst always remained inside the reactor. In this way, the catalyst was always exposed to a high hydrogen pressure, which resulted in an extended catalyst lifetime. In other words, a low hydrogen concentration inside the catalyst leads to deactivation, which can be prevented by minimizing the diffusion distance inside the catalyst. (iii) The solvent is not completely inert and may lead to unwanted side reactions, although these side

* Corresponding author. Tel.: +31 15 278 90 84; fax: +31 15 278 50 06.
E-mail address: kreutzer@tnw.tudelft.nl (M.T. Kreutzer).

0920-5861/$ – see front matter © 2005 Elsevier B.V. All rights reserved.
doi:10.1016/j.cattod.2005.06.028

Nomenclature

a	interfacial area (m^{-1})
Bo	Bodenstein number ($=uL/D_{ax}$)
c	concentration (mol/m^3)
Ca	capillary number ($=\mu_L u/\gamma$)
C_p	specific heat (kJ/(kg K))
D	diffusion coefficient (m^2/s)
D_{ax}	dispersion coefficient (m^2/s)
D_{eff}	diffusion coefficient in catalyst (m^2/s)
d_{ch}	channel diameter (m)
d_{wc}	washcoat thickness (m)
E_A	activation energy (kJ/mol)
ΔH_R	heat of reaction (kJ/mol)
ΔH_j	heat of absorption of component j (kJ/mol)
k	mass transfer coefficient (m/s)
k	reaction rate constant ($m^{3/2}$/(mol$^{1/2}$ s))
K	absorption constant (m^3/mol)
L	length (m)
L^*_{slug}	slug aspect ratio ($=L_{slug}/d_{ch}$)
N_R	number of reactions
p	pressure (Pa)
r	washcoat layer coordinate (m)
r_V	reaction rate (mol/(m^3 s))
R	gas constant (J/(mol K))
Sh	Sherwood number ($=kd/D$)
t	time (s)
T	temperature (K)
u	velocity (m/s)
U	two-phase superficial velocity (m/s)
u_{Gs}	superficial gas velocity (m/s)
u_{Ls}	superficial liquid velocity (m/s)
V	volume (m^3)
z	axial coordinate (m)

Greek letters

δ	film thickness (m)
ϵ_L	liquid holdup (m^3/m^3)
ϵ_G	gas holdup (m^3/m^3)
ϕ	flow rate (m^3/s)
γ	surface tension (N/m)
μ	viscosity (Pa s)
ρ	density (kg/m^3)
τ	mean residence time from E-curve (s)
ξ	conversion

reactions can be suppressed by adding carbon monoxide to the gas feed [5]. (iv) Heat removal from the reaction medium and hydrogen supply to the catalyst are coupled in stirred tank reactors. In other words, a temperature excursion cannot be controlled by switching the stirrer off: although the supply of hydrogen to the catalyst stops, the heat removal also stops. A possible solution to this problem is operating the process in such a way that the heat of reaction can be removed outside of the reactor.

2. Monolith loop reactor

Machado et al. [2] have proposed a loop reactor with monolithic catalysts for the DNT hydrogenation. In the proposed reactor, the product 24TDA is used as the solvent, so no solvent separation is necessary. 24TDA has a melting point of 371 K, and if the product is to be used as a liquid solvent, the operating temperature must be higher than 371 K. The upper limit for the operating temperature depends on the rate of unwanted side reactions. At temperatures above 430 K, dinitrotoluene starts to decompose, leading to a strong temperature rise which may lead to an explosion. Within the desired temperature limits 375–430 K, the vapour pressure of 24TDA is below 1 kPa, and product evaporation may be ignored. This simplifies the reactor modelling: the integral heat balance reduces to

$$\phi_L \rho C_p \Delta T = \phi_L (2\Delta H_R \xi_{NO_2}) c_{DNT,0} \quad (1)$$

In Eq. (1), ΔT is the temperature rise of the liquid stream (flowrate ϕ_L) in the reactor, ρ and C_p the liquid density and heat capacity, respectively, ξ_{NO_2} the fraction of nitro-groups converted, ΔH_R the heat of reaction per nitro-group and $c_{DNT,0}$ is the DNT feed concentration. The left hand side is the amount of heat absorbed by the product stream per unit cross sectional area of the column, and the right hand side is the amount of heat produced by reaction. In the loop reactor concept, the product stream is cooled by an external heat exchanger. Part of the cooled product stream is returned to the reactor after addition of fresh reactant. The rest of the product stream leaves the process. So, for 24DNT the loop is a single pass reactor at full conversion, and only the product is recycled in the loop. If the loop reactor is operated at lower than 100% conversion, a small finishing reactor can be added here. Of course, exotherms are not a problem for the finishing reactor at low concentrations. The entire process is depicted schematically in Fig. 1.

As stated above, in a slurry reactor, the heat transfer characteristics and the mass transfer characteristics are coupled via the intensity of stirring. The use of an external heat exchanger effectively decouples the heat removal from the gas–liquid contacting and leads to more operational flexibility.

The concept of a loop reactor with an external heat exchanger has been proposed before. Zarnack et al. [6] proposed a *venturi loop reactor* with an external heat exchanger for a solvent free DNT hydrogenation process. Apart from avoiding a solvent separation step, the use of 24TDA as a solvent was motivated by the possibility to operate the process at the highest allowable temperature, so a significant amount of the heat produced can be recovered as high temperature steam. Venturi ejectors are devices that use the kinetic energy of a high velocity liquid jet to suck in and disperse gas. A high amount of energy can be dissipated with a venturi ejector, resulting in high mass transfer in the turbulent bubble dispersion in the draft tube below the

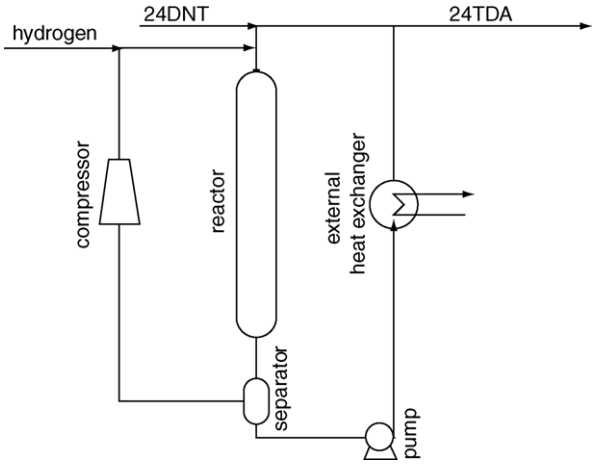

Fig. 1. Flow sheet of a monolith loop reactor for the hydrogenation of 2,4-dinitrotoluene. Adapted from Machado et al. [2].

venturi see e.g. [7,8]. In the process proposed by Zarnack et al., a venturi ejector vigorously mixes the hydrogen and liquid stream, which are allowed to react further in a large vessel that is stirred by the jet leaving the venturi. In short, a venturi loop reactor is a back-mixed reactor with good mass transfer characteristics. The catalyst in this reactor is a finely dispersed powder, and this powder still has to be separated from the product stream. For a maximum temperature rise of 10 K at full conversion in the reactor, the ratio of dinitrotoluene mass flow rate to recycle mass flow rate was 1:180. Using Eq. (1), the product ρC_p of 24TDA can then be estimated as 3.2×10^3 kJ/(m^3 K).

The advantage of the venturi loop reactor is that no compressor is needed to recycle the gas stream. Of course the gas–liquid contacting is coupled to the liquid flow rate, but a valve in the gas recycle line between the reactor vessel and the venturi allows to shut down the gas–liquid contacting while maintaining liquid flow through the external heat exchanger. A disadvantage of the venturi loop reactor is the high energy requirement. Although in the draft tube of the ejector the mass transfer is high, the energetic cost of forcing the liquid through the nozzle is high. Note that to keep the temperature rise within the 10 K limit, on average each kilogram of produced toluene diamine is forced through this nozzle 180 times before it leaves the loop.

In comparison to the venturi loop reactor, the monolith loop reactor proposed by Machado et al. [2] exploits the plug flow characteristics and low pressure drop of monoliths, while retaining the good mass transfer characteristics. Note that it is possible to operate monoliths at zero pressure drop, but at zero pressure drop the operating conditions depend on the type of distributor used and the gas flow rate is coupled to the liquid flow rate. With a small compressor and a control valve, the gas flow rate can be set independently of the liquid flow rate. Because of the liquid recycle flow rate, the low pressure drop over the column is a crucial advantage.

3. Kinetics

The kinetics of 24DNT hydrogenation has been reported in the open literature [9–15]. The reaction is known to proceed via two intermediates 2-amino-4-nitrotoluene (2A4NT) and 4-amino-2-nitrotoluene (4A2NT) to the final product 24TDA. All agree that the hydrogenation of the nitro-group opposite of the methyl group is faster than the hydrogenation of the sterically hindered nitro-group next to the methyl group. All kinetic studies were performed at temperatures, lower than the boiling point of 24TDA in solvents such as ethyl acetate and methanol. As a result, for this work we have to extrapolate the kinetics to higher temperatures using the heat of adsorption of the components and the activation energy for the individual reactions.

In this study, the kinetic constants of Malyala and Chaudhari [15] at 333 K for a Nickel catalyst were used. All the kinetic parameters are listed in Table 1. The volumetric rate of the individual reactions follows Langmuir–Hinshelwood kinetics, where the rate limiting step is a reaction of adsorbed dissociated hydrogen with a nitro-aromatic compound. Following the kinetics of Malyala and Chaudhari [15], the adsorption of the sterically hindered nitro-group in 2A4NT and the adsorption of the reaction product 24TDA may be ignored in the site balance. Numbering the reactions as shown in Fig. 2, the rate expressions are given by

$$r_{V,1} = \frac{k_1 \sqrt{c_H} c_A}{\left(1 + \sqrt{K_H c_H} + K_A c_A + K_B c_B\right)^2} \quad (2)$$

$$r_{V,2} = \frac{k_2 \sqrt{c_H} c_A}{\left(1 + \sqrt{K_H c_H} + K_A c_A + K_B c_B\right)^2} \quad (3)$$

$$r_{V,3} = \frac{k_3 \sqrt{c_H} c_B}{\left(1 + \sqrt{K_H c_H} + K_A c_A + K_B c_B\right)^2} \quad (4)$$

$$r_{V,4} = \frac{k_4 \sqrt{c_H} c_C}{\left(1 + \sqrt{K_H c_H} + K_A c_A + K_B c_B\right)^2} \quad (5)$$

The subscripts H, A, and B represent hydrogen, 24DNT and 4A2NT, respectively.

The temperature dependency of the rate constants k_i and the adsorption coefficients K_j are given by the Arrhenius

Table 1
Kinetic parameters

i	k_i (333 K) (m^3/(mol s))	$E_{A,i}$ (kJ/mol)
1	5.20×10^{-2}	30.7
2	6.88×10^{-3}	33.2
3	8.54×10^{-3}	31.0
4	4.68×10^{-3}	33.8

j	K_j (333 K) (m^3/mol)	ΔH_j (kJ/mol)
H_2	9.36×10^{-4}	−34.07
24DNT	1.11×10^{-2}	−14.11
4A2NT	9.80×10^{-4}	−12.19

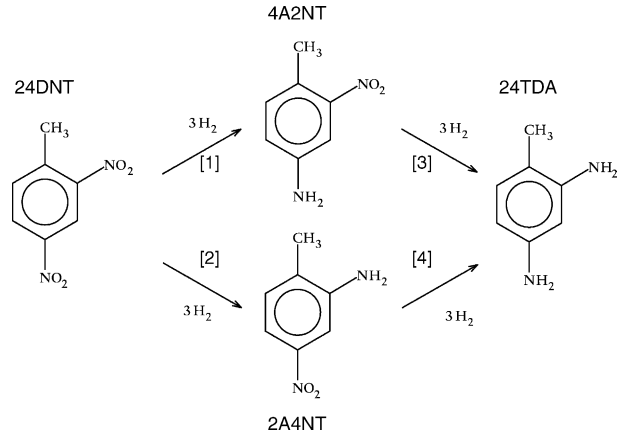

Fig. 2. Reaction pathway for the hydrogenation of 2,4-dinitrotoluene (24DNT) to the intermediates 2-amino-4-nitrotoluene (2A4NT) and 4-animo-2-nitrotoluene (4A2NT) and subsequently to the product 2,4-toluenediamine. The numbers between brackets are the labels by which the reactions are referred to in the text.

equations

$$k_i(T) = k_i(T_{\text{ref}})\exp\left[\frac{-E_A}{R}\left(\frac{1}{T}-\frac{1}{T_{\text{ref}}}\right)\right] \quad (6)$$

$$K_j(T) = K_j(T_{\text{ref}})\exp\left[\frac{-\Delta H_j}{R}\left(\frac{1}{T}-\frac{1}{T_{\text{ref}}}\right)\right] \quad (7)$$

4. Reactor model

The partial differential equations describing the cocurrent multiphase monolith reactor are listed in Table 5. The assumptions of the model are summarised in Table 2.

For the liquid phase component balance, the terms on the right hand side are the convective term, the dispersion term and the mass transfer to the catalyst. Maldistribution is taken into account by a dispersion term [16].

The balance for the gas phase is only set up for hydrogen. The pressure drop is low with respect to the operating pressure, and the gas-phase concentration p/RT is assumed to be constant in the reactor. Although the concentrations are constant, the balance needs to be solve to determine the reduction in volumetric gas flow. The left hand side is derived by

$$\frac{\partial \epsilon_G c_{H,g}}{\partial t} = \frac{p}{RT}\frac{u_{Ls}}{U^2}\frac{\partial u_{Gs}}{\partial t} - \epsilon_G \frac{p}{RT^2}\frac{\partial T}{\partial t} \quad (8)$$

in which we have used the ideal gas law $c_{H,g} = p/RT$ and $\epsilon_G = u_{Gs}/U$. For the right hand side, the following derivation applies:

$$\frac{\partial u_{Gs} c_{H,g}}{\partial z} = -\frac{p}{RT}\frac{\partial u_{Gs}}{\partial z} - \frac{u_{Gs}\, p}{RT^2}\frac{\partial T}{\partial z} \quad (9)$$

The right hand side of the enthalpy balance consists of a convective term, and a reactive term. For the reactive term, we have used the fact that the mass transfer of water from the catalyst equals the reaction rate inside the catalyst, and the fact that per mol nitro-group converted 2 mol of water is formed. The heat of reaction in the enthalpy balance is defined per mol nitro-group ($-\Delta H_R = 550$ kJ/mol).

Finally, inside the catalyst the mass balance has a diffusive term and a reactive term. For the effective diffusion coefficient inside the catalyst we have assumed $D_{\text{eff}} = 0.1D$. The boundary condition at the washcoat–liquid interface couples the liquid and gas axial balances to the internal balances, and reflects that the reaction rate in the catalyst equals the flux to the catalyst.

The mass transfer parameters are given in Table 3. For the transfer for non-volatile components to the catalyst, the correlation for developed flow from [17] was used, in series with the resistance in the film. Note that this resistance-in-series model is a lower estimate for this mass transfer step. For the transfer of hydrogen to the catalyst, the hydrogen concentration in the slugs was calculated with the correlation developed in [17]. Two types of channel shapes were considered: round channels and channels with rounded

Table 2
Model assumptions

No catalyst deactivation
No internal temperature gradients
No evaporation of liquid phase components
No homogeneous reactions
No side reactions
Maldistribution may be taken into account by axial dispersion in the liquid phase
Gas and liquid temperature in equilibrium

Table 3
Mass transfer model

$U = u_{Ls} + u_{Gs}, \quad \epsilon_L = \frac{u_{Ls}}{U}, \quad \epsilon_G = \frac{u_{Gs}}{U}, \quad Ca = \frac{\mu U}{\gamma}$

Film thickness

$\delta = d_{ch}\frac{0.66Ca^{2/3}}{1+3.33Ca^{2/3}}$
(round channels)
$\delta = 3d_{ch}\left(\frac{1}{2} - [0.64 + 0.36\exp(-3.08Ca^{0.54})]\right)$
(rounded channels)

Liquid-to-catalyst

$Sh = 90 + 104\left(\frac{L_{slug}}{d_{ch}}\right)^{-4/3}$
$k_{LS} = \epsilon_L\left(\frac{\delta}{D} + \frac{d_{ch}}{ShD}\right)^{-1}, \qquad k_{LS}a = k_{LS}\frac{4}{d_{ch}}$

Gas-to-catalyst (direct)

$k_{GS} = \epsilon_G\frac{D}{\delta}, \qquad k_{LS}a = k_{GS}\frac{4}{d_{ch}}$

Gas-to-catalyst (through slugs)

$k_{GLS} = \epsilon_L\frac{D}{\delta}, \qquad k_{GLS}a = k_{GLS}\frac{4}{d_{ch}}$
$c_{H,slug} = c_{H,sat}\left(1 + \frac{L_{slug}}{\delta}\sqrt{\frac{D\pi}{8Ud_{ch}}}\right)^{-1}$

Table 4
Physical properties

Hydrogen	
Henry coefficient	0.44 mol/(m^3 bar)
Diffusion coefficient (383 K)	2.3×10^{-8} m^2/s
Diffusion coefficient (433 K)	5.9×10^{-8} m^2/s
Water	
Diffusion coefficient (383 K)	7.5×10^{-9} m^2/s
Diffusion coefficient (433 K)	1.9×10^{-8} m^2/s
24TDA	
Density	1020 kg/m^3
Viscosity (383 K)	7.4×10^{-4} Pa s
Viscosity (433 K)	3.2×10^{-4} Pa s
Surface tension	4.2×10^{-2} N/m
Heat capacity	3.1 kJ/(kg K)
24DNT, 2A4NT, 4A2NT, TDA	
Diffusion coefficient (383 K)	1.9×10^{-9} m^2/s
Diffusion coefficient (433 K)	4.9×10^{-9} m^2/s

corners. For round channels, the low inertia correlation of Aussilous and Quéré [18] was used to estimate the film thickness, and for rounded channels three times the film thickness predicted by the correlation of Irandoust and Andersson [19] was used, based on the experimental mass transfer rates obtained in [20].

The heat capacity of 24TDA and the solubility of hydrogen in 24TDA are reported by Zarnack et al. [6]. The viscosity, surface tension and density of 24TDA were taken from Yaws [21]. Because the temperature rise in the column may be significant, the viscosity of 24TDA cannot be assumed to be constant in the column. The viscosity was calculated at each axial position inside the column as a function of temperature. The diffusion coefficients were estimated using the Wilke-Chang correlation [22]. Since the diffusion coefficients predicted by this correlation are a strong function of viscosity, the diffusion coefficients were also calculated at each axial position. An overview of the physical properties is given in Table 4.

The partial differential equations in Table 5 were discretised using the finite difference DSS/2 routines [23] on a 2D grid of typically 50 points in the axial direction and 15 points in the radial (washcoat) direction.

The initial conditions for the simulation was that all variables were equal to the feed conditions.

$$u_{\mathrm{Gs}} = u_{\mathrm{G,in}}, \qquad T = T_{\mathrm{in}}, \qquad c_{\mathrm{L}} = c_{\mathrm{S}} = c_{\mathrm{L,in}} \tag{10}$$

The resulting ODE's were integrated using the LSODES integrator [24] until steady-state was reached.

5. Results

As a base case, we have performed the simulations for a column with a volume of 1 m^3 and a height of 5 m. The monoliths channels are assumed to be coated in such a way that channel cross section is round with a diameter of 1.1 mm (400 cpsi), and such that the washcoat (10% Ni–Y) thickness is 25 μm. The optimal feed concentration was calculated from the allowable temperature rise, taken to be

Table 5
Differential equations and boundary conditions for the mass and enthalpy balances in the reactor

Liquid-phase mass balances for non-volatile components (i = 24DNT, 4A2NT, 2A4NT, 24TDA, H_2O)

$$\epsilon_{\mathrm{L}} \frac{\partial c_{\mathrm{L},i}}{\partial t} = -u_{\mathrm{Ls}} \frac{\partial c_{\mathrm{L},i}}{\partial z} + D_{\mathrm{ax}} \frac{\partial^2 c_{\mathrm{L},i}}{\partial z^2} - k_{\mathrm{LS}} a_i (c_{\mathrm{L},i} - c_{\mathrm{S},i})$$

$$\left.\frac{\partial c_{\mathrm{L},i}}{\partial z}\right|_{z=0} = \frac{u_{\mathrm{Ls}}}{D_{\mathrm{ax}}} (c_{\mathrm{L},i} - c_{\mathrm{L},i,\mathrm{in}}), \qquad \left.\frac{\partial c_{\mathrm{L},i}}{\partial z}\right|_{z=L} = 0$$

Gas-phase hydrogen mass balance

$$\frac{p}{RT}\frac{u_{\mathrm{Ls}}}{U^2}\frac{\partial u_{\mathrm{Gs}}}{\partial t} - \frac{\epsilon_{\mathrm{G}}\, p}{RT^2}\frac{\partial T}{\partial t} = -\frac{p}{RT}\frac{\partial u_{\mathrm{Gs}}}{\partial z} + \frac{u_{\mathrm{Gs}}\, p}{RT^2}\frac{\partial T}{\partial z} + k_{\mathrm{GLS}} a (c_{\mathrm{H,slug}} - c_{\mathrm{S}}) + k_{\mathrm{GS}} a (c^* - c_{\mathrm{S}})$$

$$u_{\mathrm{Gs}}|_{z=0} = u_{\mathrm{G,s,in}}$$

Enthalpy balance

$$\epsilon_{\mathrm{L}} \rho C_{\mathrm{p}} \frac{\partial T}{\partial t} = -u_{\mathrm{Ls}} \rho C_{\mathrm{p}} \frac{\partial T}{\partial t} - \tfrac{1}{2} \Delta H_{\mathrm{R}} [k_{\mathrm{LS}} a (c_{\mathrm{L}} - c_{\mathrm{S}})] \mathrm{H_2O}$$

$$T|_{z=0} = T_{\mathrm{in}}$$

Washcoat mass balance for component i

$$\frac{\partial c_i}{\partial r} = D_{\mathrm{eff}} \frac{\partial^2 c_i}{\partial r^2} + \sum_{j=1}^{N_{\mathrm{R}}} v_{i,j} r_{\mathrm{V},j}$$

$$D_{\mathrm{eff}} \left.\frac{\partial c_i}{\partial r}\right|_{r=d_{\mathrm{wc}}} = k_{\mathrm{LS}} (c_{\mathrm{L},i} - c_{\mathrm{S},i}), \qquad \left.\frac{\partial c_i}{\partial r}\right|_{r=0} = 0 \text{ (non-volatile)}$$

$$D_{\mathrm{eff}} \left.\frac{\partial c_i}{\partial r}\right|_{r=d_{\mathrm{wc}}} = k_{\mathrm{GS}} (c^* - c_{\mathrm{S}}) + k_{\mathrm{GLS}} (c_{\mathrm{H,slug}} - c_{\mathrm{S}}), \qquad \left.\frac{\partial c_i}{\partial r}\right|_{r=0} = 0 \ (\mathrm{H_2})$$

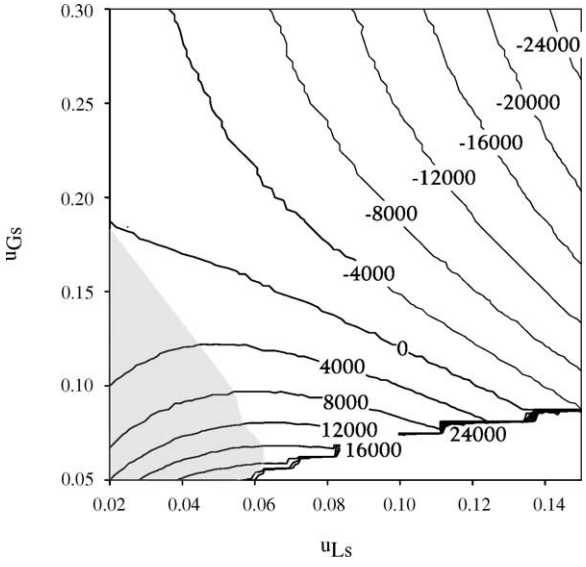

Fig. 3. Pressure drop contour map for the hydrogenation of 24DNT. Round channels with d_{ch} = 1.1 mm. The numbers for each line give the pressure drop in Pa, where positive numbers indicate that the pressure on top of the column is higher than at the bottom. L_{col} = 5 m, p_{in} = 32 bar, T_{in} = 383 K, 24DNT feed concentration is 140 mol/m^3.

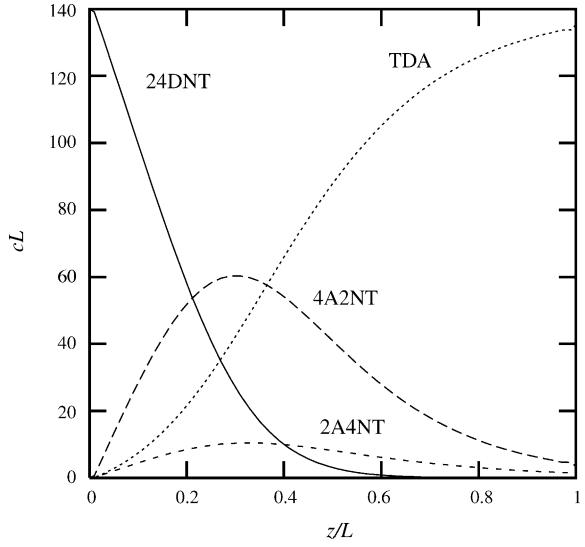

Fig. 4. Concentration profile of the aromatic components in a 5 m long 400 cpsi monolith reactor with a washcoat of 25 μm. u_{Ls} = 4 cm/s u_{Gs} = 10 cm/s, T_{in} = 383 K, 24DNT feed concentration is 140 mol/m^3.

50 K (from 383 to 433 K).

$$c_{DNT,0} = \frac{1000\,\mathrm{kJ/m^3} \times 3.1\,\mathrm{kJ/kg/K} \times 50\,\mathrm{K}}{2 \times 550\,\mathrm{kJ/mol}} = 140\,\mathrm{mol/m^3} \quad (11)$$

Kreutzer et al. [16] formulated hydrodynamic stability criteria for monoliths. Briefly, the flow is stable if the pressure drop increases with an increase of u_{Ls} or u_{Gs}. Due to reaction, the gas velocity decreases and the temperature dependent fluid properties change, so the pressure drop was calculated using the friction factor correlation from [25],

$$f = \frac{16}{Re}\left[1 + 0.17\frac{1}{L^*_{slug}}\left(\frac{Re}{Ca}\right)^{0.33}\right], \quad (12)$$

at each axial position in the column, and integrated over the reactor length to obtain the pressure drop over the column. In Fig. 3, the contour lines of pressure drop versus u_{Ls} and u_{Gs} are plotted. Using as stability criterion that the pressure drop must increase with an increase of u_{Ls} or u_{Gs}, the system is stable above ($u_{Ls} \approx 0.04$, $u_{Gs} \approx 0.12$), ($u_{Ls} \approx 0.06$, $u_{Gs} \approx 0.07$), and for all liquid velocities if the gas velocity is higher than 0.17.

If the liquid superficial velocity is 0.04 m/s and we set the gas inlet superficial velocity to 0.1 m/s, then the stoichiometric minimum hydrogen pressure needed to completely hydrogenate all DNT is 11 bar. Inside the column, the bubbles shrink due to the hydrogen consumption, and operating the reactor at somewhat higher pressures ensures that the bubbles retain their elongated shape, ensuring Taylor flow over the entire column. Finally, maldistributions were taken into account using a Bodenstein number $Bo = UL/D_{ax}$ of 100 per meter column and a column length of 5 m, and we

Table 6
DNT conversion, TDA yield and outlet temperature for several simulations

Run	u_{Ls} (m/s)	u_{Gs} (m/s)	$c_{DNT,in}$ (mol/m^3)	T_{in} (K)	p (bar)	L_{col} (m)	d_{wc} (μm)	d_{ch} (mm)	Shape*	Pe	Conversion DNT	Yield TDA	T_{out} (K)
1	0.04	0.10	040	383	16	5	25	1.1	Circ.	500	100.0	96.42	431.7
2	0.04	0.10	70	383	16	5	25	1.1	Circ.	500	99.90	87.95	406.2
3	0.04	0.10	70	403	16	5	25	1.1	Circ.	500	100.0	97.50	427.5
4	0.04	0.10	140	383	16	5	25	1.1	Circ.	100	99.98	94.34	431.2
5	0.04	0.10	140	383	16	5.5	25	1.1	Circ.	100	99.99	96.16	431.7
6	0.04	0.10	140	383	32	5	25	1.1	Circ.	500	100.0	98.81	432.3
7	0.04	0.05	140	383	32	5	25	1.1	Circ.	500	100.0	99.32	432.5
8	0.04	0.10	140	383	16	5	25	0.9	Circ.	500	100.0	98.82	432.3
9	0.04	0.10	140	383	16	5	25	1.1	Rect.	500	99.80	92.90	430.6
10	0.04	0.10	140	383	32	5	25	1.1	Rect.	500	99.86	96.02	431.5
11	0.08	0.20	140	383	16	10	25	1.1	Circ.	500	100.0	96.11	431.5
12	0.04	0.10	140	383	16	5	15	1.1	Circ.	500	99.98	85.91	428.8

* Rect., rounded channels; Circ., round channels.

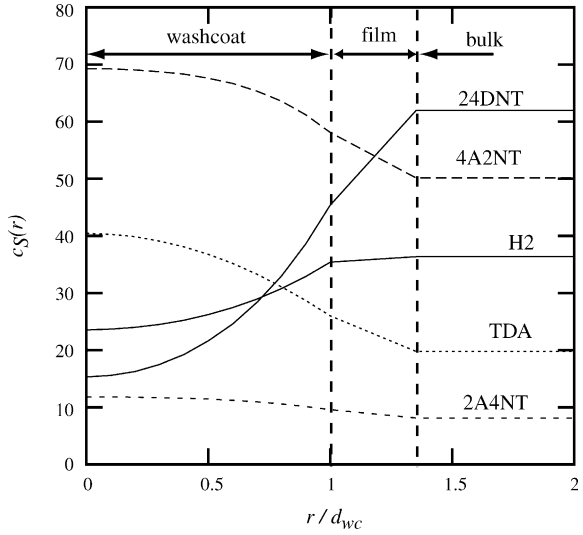

Fig. 5. Concentration profiles in the catalyst and liquid bulk at $z/L = 0.1$ for the same conditions as in Fig. 4.

have tested the impact of lowering the Bodenstein number to 20 per meter column length.

In Fig. 4 the profiles of the liquid phase in the axial direction are shown. The conversion of 24DNT, the yield of 24TDA and the outlet temperature are reported for this base case as run 1 in Table 6.

In Fig. 5, the catalyst concentration inside the catalyst, the film and the liquid bulk is plotted. Although three molecules of hydrogen are consumed in the conversion of 24DNT, the impact of reaction on the concentration profiles of 24DNT inside the catalyst and the film is more severe, because the diffusion coefficient of 24DNT is significantly lower than the diffusion coefficient of hydrogen. A high hydrogen concentration inside the catalyst prevents deactivation, the obtained profiles are beneficial for the stability of the catalyst.

With increasing conversion, the temperature rises and the viscosity of the liquid drops. As a result, the thickness of the film between the bubbles and the slugs is reduced, and the temperature rise decreases the external mass transfer limitations close to full conversion.

In Table 6, the temperature rise, 24DNT conversion and 24TDA yield are given for several simulations. Run 2 demonstrates the effect of operating the reactor at a lower feed concentration. Although lowering the concentrations of aromatic compounds reduces the driving force for mass transfer to the catalyst, the main reason for the lower yield to 24TDA is that the temperature rise is lower and the high reaction rates associated with high temperatures are not obtained. Run 3 shows the effect of increasing the higher feed temperature at low feed concentrations. Now the feed temperature is high enough to ''kick off'' the reaction, and the TDA yield is comparable to the process at higher concentration.

Run 4 shows the effect of more severe maldistribution: reducing the Bodenstein number by a factor 5 lowers the yield and even the conversion of 24DNT. For this higher extent of maldistribution, a 10% increase in column length is required to obtain roughly the same yield and conversion, as is shown in run 5. Since the hydrogenation must run to completion, the impact of maldistribution can be overcome by using a longer reactor.

Run 6 shows the effect of increasing the reaction pressure. At higher pressure, the rate of reaction increases, but the residence time of the liquid inside the column is decreased. A lower fraction of the gas is consumed, and as a result, the linear velocity of the bubbles and slugs is not reduced significantly inside the column. As a result, only a slightly higher yield for TDA is found. In run 7, the pressure is increased and the gas superficial velocity is decreased, so the molar feed of hydrogen is equal to the base case run 1. As a result, the yield is substantially higher.

Runs 8 and 9 demonstrate the effect of catalyst geometry: increasing the cell density to 600 cpsi (run 8) improves the yield of 24TDA and using a coating that is not perfectly round (run 9) reduces yield significantly. The effect of using channels that are not perfectly round leads to more severe mass transfer limitations, and can overcome by increasing the pressure (run 10). The reaction is not severely limited by external mass transfer. Increasing the superficial velocities results in a higher film thickness. In run 11 increasing the superficial velocities while keeping the residence time constant only results in a very minor decrease in yield.

Finally, run 12 demonstrates the effect of using a thinner washcoat. Since the mass transfer limitations were not severe for a washcoat of 25 μm (see Fig. 5), reducing the washcoat thickness reduces the yield significantly.

6. Discussion

A direct comparison of the simulations presented in this work to the data in the patent of Machado et al. [2] is impossible: the catalyst used by Machado et al. [2] is a 1%Pd/10%Ni/γ-Al_2O_3 catalyst which is different from the catalyst used to measure the kinetic equations used in this work. However, several of the trends are the same. Machado et al. found that increasing the gas–liquid mass transfer had a negligible effect on the conversion and yield, which is consistent with the observation that the slugs are practically saturated with hydrogen. Machado et al. also found that the yield increases with pressure, although that result would be obtained using any of the kinetics in the open literature. Machado et al. did not find a decrease in yield for lower feed concentrations, which suggests that their Pd-based catalyst has a higher activation energy, so the reactor ''kicks off'' at lower temperatures. Malyala et al. [13] reported such higher activation energies for a Pd-based catalysts. Also, in this work internal and external temperature gradients were not considered. The heat of reaction may lead to such a gradient, which would also result in a lower ''kick-off'' temperature.

The stability criteria that were found in this study are valid for 400 cpsi. If higher cell densities are used, monoliths

can be operated at even lower velocities, which would allow a further decrease in reactor size. Note that the mass transfer characteristics improve for higher cell densities and for lower velocities.

No explicit comparison has been made with stirred tank reactors or other fixed bed reactors in this study. However, several remarks can be made in comparison. Stirred tank reactors are backmixed, so a higher reactor volume is required. An interesting observation can be made with respect to operational safety. If in the monolith loop reactor the liquid feed is stopped, and the gas feed is switched from hydrogen to nitrogen, the reaction stops in a time that is equal to the residence time in the reactor. For the base case considered in this study, the residence time is 33 s. In other words, monoliths can be emptied quickly in the event of a temperature excursion. In a large stirred tank, the hydrogen gas phase is also backmixed and does not leave the reactor as fast, so such an abrupt stop is not possible.

With respect to trickle bed reactors, that are prone to stagnant zones that lead to hot spots, a similar remark can be made. Further, the attainable mass transfer rates in trickle beds are much lower. Although the stability problems associated with hydrogen depletion inside the catalyst can be overcome by using egg-shell catalysts, due to liquid–solid mass transfer limitations the required reactor volume for a trickle bed remains very high.

7. Conclusions

In this work, a design for the industrially relevant hydrogenation of 2,4-dinitrotoluene using a monolith loop reactor has been presented. The monolith loop reactor eliminates the disadvantages of other configurations, such as separation of solvent and/or catalyst, deactivation due to catalyst separation outside the reactor and side reactions with solvents. The main advantages of using a monolith for this process are:

- Low pressure drop, which is especially beneficial because of the high recycle ratio.
- High mass transfer, which reduces reactor volume and deactivation.
- Plug flow. Although the reaction runs to completion, the reaction can be carried out in a small reactor because of the limited extent of backmixing in monolith reactors.

The design is based on the results for pressure drop, residence time distribution and mass transfer presented in [16,17,25].

The optimal operating conditions are largely determined by the hydrodynamic stability. Reducing the superficial gas and liquid velocities increases the residence time and improves the mass transfer, so the column should be operated at the lowest possible superficial velocities, which can be found from a hydrodynamic stability analysis.

References

[1] M.T. Kreutzer, F. Kapteijn, J.A. Moulijn, J.J. Heisz-wolf, Chem. Eng. Sci. 25 (2005) 2155–2159.
[2] R.M. Machado, D.J. Parrillo, R.P. Boehme, R.R. Broekhuis, U.S. Patent 6,005,143 (1999).
[3] H.J. Janssen, H.J. Vos, K.R. Westerterp, Chem. Eng. Sci. 47 (1992) 4191–4208.
[4] J.J. Chimerol, W.M. Clarke, W.I. Denton, P.D. Hammond, German Patent DE 1,518,080 (1965).
[5] S.K. Bhutani, U.S. Patent 3,935,264 (1976).
[6] U.J. Zarnack, F. Pohl, D. Grenner, H. Hetzel, H. Judat, 5,563,296 (1996).
[7] P.H.M.R. Cramers, A.A.C.M. Beenackers, L.L. van Dierendonck, Chem. Eng. Sci. 47 (1992) 3557–3564.
[8] P.H.M.R. Cramers, A.A.C.M. Beenackers, Chem. Eng. J. 82 (2001) 131–141.
[9] H.J. Janssen, A.J. Kruithof, G.J. Steghuis, K.R. Westerterp, Ind. Eng. Chem. Res. 29 (1990) 754–766.
[10] H.J. Janssen, A.J. Kruithof, G.J. Steghuis, K.R. Westerterp, Ind. Eng. Chem. Res. 29 (1990) 1822–1829.
[11] E.J. Molga, K.R. Westerterp, Chem. Eng. Sci. 47 (1992) 1733–1949.
[12] G. Neri, M.G. Musolino, C. Milone, S. Galvagno, Ind. Eng. Chem. Res. 34 (1995) 2226–2231.
[13] R.V. Malyala, D.D. Nikalje, R. Jaganathan, R. Chaudhari, Ind. Eng. Chem. Res. 36 (1997) 592–604.
[14] R.V. Malyala, R. Jaganathan, R.V. Chaudhari, Chem. Eng. Sci. 53 (1998) 787–805.
[15] R.V. Malyala, R.V. Chaudhari, Ind. Eng. Chem. Res. 38 (1999) 906–915.
[16] M.T. Kreutzer, J.J.W. Bakker, F. Kapteijn, J.A. Moulijn, P.J.T. Verheijen, Ind. Eng. Chem. Res. doi: 10.1021/ie0492350, in press.
[17] M.T. Kreutzer, Hydrodynamics of Taylor flow in capillaries and monoliths channels, Doctoral Dissertation, Delft University of Technology, Delft, The Netherlands, 2003.
[18] P. Aussilous, D. Quere, Phys. Fluids 12 (2000) 2367–2371.
[19] S. Irandoust, B. Andersson, Ind. Eng. Chem. Res. 28 (1989) 1684.
[20] M.T. Kreutzer, P. Du, J.J. Heiszwolf, F. Kapteijn, J.A. Moulijn, Chem. Eng. Sci. 56 (2001) 6015–6023.
[21] C.L. Yaws, Chemical Properties Handbook, McGraw-Hill, New York, 1999.
[22] R.R. Reid, J.M. Prausnitz, B.E. Poling, The Properties of Gasses and Liquids, fourth ed., McGraw-Hill, New York, 1987.
[23] W.E. Schiesser, The Numerical Method of Lines—Integration of Partial Differential Equations, Academic Press, San Diego, CA, USA, 1991.
[24] A.C. Hindmarsh, in: R.S. Stepleman (Ed.), Scientific Computing, Applications of Mathematics and Computing to the Physical Sciences, IMACS Transactions on Scientific Computation, vol. 1, Elsevier Science Ltd., Amsterdam, 1983, pp. 55–64.
[25] M.T. Kreutzer, F. Kapteijn, J.A. Moulijn, C.R. Kleijn, AIChE J., doi:10.1002/aic.10495.